Engineering Geology 367 (2026) 108702

Contents lists available at ScienceDirect

Engineering Geology

journal homepage: www.elsevier.com/locate/enggeo

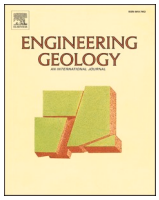

A combined field and laboratory investigation into the moisture dependency of V_s for a clay-rich railway embankment fill

Qasim Khan [a], Muhammad Saqlain [a,*], Andrew Trafford [a], Ben Dashwood [b], J.E. Chambers [b], Gavin Jessamy [c], Julian Harms [c], Shane Donohue [a]

[a] School of Civil Engineering, University College Dublin, Dublin, Ireland
[b] British Geological Survey, UK
[c] Network Rail, UK

ARTICLE INFO

Keywords:
Partially saturated soils
Clay soils
Shear wave velocity
Small-strain stiffness
Geophysical monitoring

ABSTRACT

Embankments that were constructed over 100 years ago in the UK are increasingly vulnerable to the impact of climate change. These embankments were constructed without standard compaction techniques and many are comprised of clay. The clay fill used in these embankments historically exhibited volumetric instability due to moisture variation. With climate change models projecting increased precipitation events in UK and Northern Europe, these embankments face a growing risk associated with their stability and serviceability. Consequently, establishing geophysical-geotechnical relationships through combined field and laboratory monitoring becomes necessary for characterising the moisture-dependent behaviour of embankments. Since V_s is related to the soil stiffness, combined field and laboratory based geophysical monitoring can help assess and understand the embankment condition under varying moisture levels. Combined field and laboratory investigations that capture the moisture-dependent behaviour of clay embankments remain limited, particularly where geophysical responses are monitored under actual environmental conditions. This study addresses that gap by examining a railway embankment constructed from London Clay through a combined field and laboratory characterisation programme designed to evaluate the influence of moisture variation on its geophysical and geotechnical properties. In the field, V_s measurements were obtained on four occasions using the Multichannel Analysis of Surface Waves (MASW) method and correlated with soil suction and moisture data recorded by sensors installed within the embankment. Complementary laboratory testing was carried out on reconstituted soil samples subjected to drying and wetting (D/W) cycles that reflected the *in-situ* suction range, enabling a controlled assessment of corresponding V_s measurements. The laboratory response was then compared with *in-situ* geophysical measurements to assess their relationship. By establishing these links, the study demonstrates the relevance and necessity of integrated field-laboratory geophysical approaches for characterising the moisture-dependent behaviour of clay embankments, particularly those susceptible to seasonal or climate-induced instability.

1. Introduction

The performance and stability of railway embankments are of significant concern in the UK, particularly in regions where high-plasticity clay soils are prevalent. Clays, such as London, Gault, Weald, Oxford, Kimmeridge and Reading, exhibit high volumetric instability, resulting in increased risk to performance of embankments constructed with them (Driscoll, 1983). Climate change poses additional risks to the stability and serviceability of these structures. Future projections suggest that the UK will experience drier summers and wetter winters, with increased temperatures accelerating evaporation and evapotranspiration rates (Hulme, 2002; Clarke and Smethurst, 2010). Furthermore, repeated drying and wetting cycles during summers and winters exacerbate these challenges, leading to considerable ground displacements in some locations (Biddle, 2001), which may necessitate imposition of speed restrictions and increased maintenance frequencies (Rail and Rail Safety

* Corresponding author.
E-mail addresses: qasim.khan@ucd.ie (Q. Khan), muhammad.saqlain@ucdconnect.ie (M. Saqlain), andrew.trafford1@ucd.ie (A. Trafford), bendas@bgs.ac.uk (B. Dashwood), jecha@bgs.ac.uk (J.E. Chambers), Gavin.Jessamy@networkrail.co.uk (G. Jessamy), Julian.Harms@networkrail.co.uk (J. Harms), shane.donohue@ucd.ie (S. Donohue).

https://doi.org/10.1016/j.enggeo.2026.108702
Received 19 June 2025; Received in revised form 13 February 2026; Accepted 18 March 2026
Available online 23 March 2026

and Standards Board (RSSB), 2011; Rail, 2018). Climate change is expected to intensify the seasonal cycles of moisture content and pore water pressure in clay soils, exacerbating problems such as shrink-swell cycles and potentially leading to more frequent and severe structural damage (Vaughan et al., 2004; Nyambayo et al., 2004). The phenomenon of hydraulic hysteresis, where the soil-water retention properties vary depending on whether the soil is wetting or drying, further complicates the prediction and management of these risks (Fredlund et al., 2011; Fredlund and Xing, 1994; Šimůnek et al., 1999; Fredlund, 2019). Experimental studies and numerical models have demonstrated that cyclic changes in moisture and stress can lead to significant movements, particularly in high-plasticity clay slopes, which are prone to progressive failure due to these environmental stress cycles (Take and Bolton, 2011; Briggs et al., 2017; Postill et al., 2020). Additionally, extreme weather events can intensify these processes, increasing future slope failure risks under changing climate conditions. These challenges highlight the need for improved monitoring strategies and predictive tools capable of capturing both spatial variability and temporal evolution in subsurface conditions within ageing railway earthworks (Rail, 2018; Holmes et al., 2022).

Seismic geophysical monitoring has shown strong potential for assessing slope and earthwork stability. In particular, multichannel analysis of surface waves (MASW) enables detailed characterisation of subsurface stiffness and related geotechnical properties (Pasquet et al., 2015; Socco et al., 2010; Bergamo et al., 2016a; Bergamo et al., 2016b; Gunn et al., 2016; Coughlan et al., 2023; Subramaniam et al., 2020; Wacquier et al., 2021; Donohue et al., 2019; Saqlain et al., 2026). The sensitivity of seismic velocity to moisture and suction variation in clays is well established (Cho and Santamarina, 2001; Donohue and Long, 2010; Dong and Lu, 2016a; Dong and Lu, 2016b; Dong et al., 2016; Walker et al., 2023), yet few site-specific studies have investigated operational railway embankments prone to moisture-induced instability and serviceability issues (Holmes et al., 2022; Bergamo et al., 2016a; Gunn et al., 2018). While these studies explored geophysical-geotechnical relationships using either seismic or resistivity monitoring, combined field and laboratory characterisation based on V_s measurements remains lacking for railway embankments. This study adopts an integrated laboratory-field approach to investigate the moisture-dependent behaviour of a soft clay railway embankment. Laboratory seismic measurements are conducted on clay samples subjected to controlled wetting and drying cycles to quantify stiffness variations associated with cyclic moisture changes. These controlled observations provide a framework for interpreting field-scale behaviour. Complementary field monitoring is undertaken at a clay filled railway embankment using Distributed Acoustic Sensing (DAS) to perform active MASW surveys at four intervals throughout the year, supported by *in-situ* soil moisture and suction instrumentation. DAS has emerged as a transformative technology in the last decade that leverages fibre optic cables to detect and measure acoustic signals through variations in Rayleigh backscattering caused by elastic vibrations (Maggio et al., 2023; Trafford et al., 2024a; Trafford et al., 2022; Soga and Luo, 2018; Fernández Ruiz et al., 2020). It is well-suited to railway embankment monitoring due to high spatio-temporal resolution and has demonstrated potential for continuous seismic monitoring using train-induced vibrations (Ouellet et al., 2024; Rossi et al., 2022; Kang et al., 2025; Thevenet et al., 2024; Shao et al., 2022). In the present study, the focus is exclusively on distinct active MASW surveys.

2. Materials and testing methods

2.1. Site description and instrumentation

The site under investigation is a c. 350 m long 4-5 m high embankment, located at Withy Beds, just North of Effingham Junction station, on Network Rail's Wessex Route, Southwest of London (Fig. 1a). This 19th century embankment has experienced issues with seasonal volume change over recent years as well as landslip on the NE side of the embankment. The embankment is constructed from reworked London Clay.

2.2. Materials and specimen preparation

Both block and remoulded samples were collected from the embankment for laboratory testing. The geotechnical index properties are provided in Table 1. Based on the liquid limit (56%) and plasticity index (31%), the soil is classified as High-Plasticity Clay with similar index properties to several other UK clays (Walker et al., 2022; Reeves et al., 2006). Portions of the collected samples were oven dried and then pulverized to pass 1 mm sieve. Any organic material, such as plant roots, were removed before oven drying. The Atterberg limits were measured

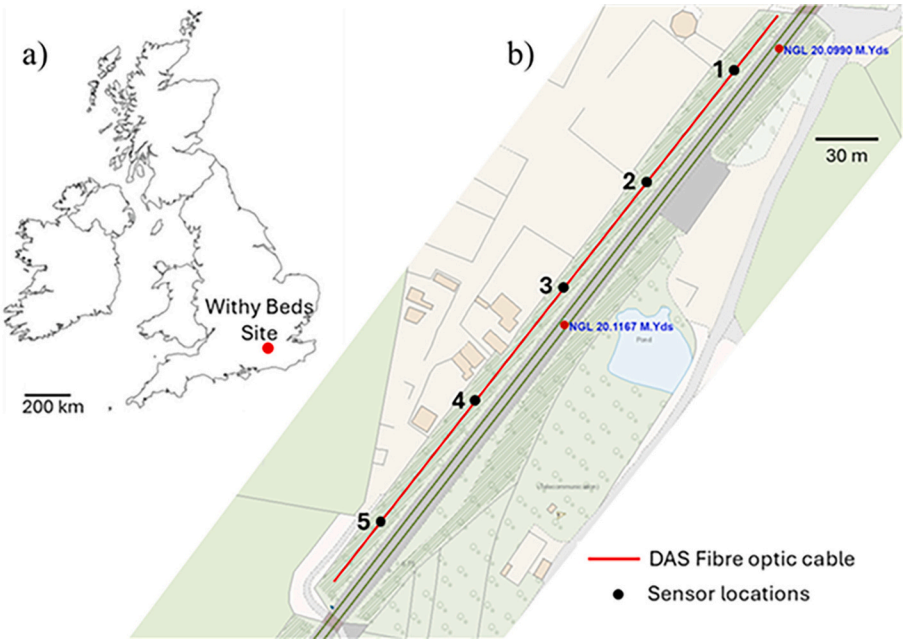

Fig. 1. Location of site and instrumentation of embankment, a) Site Map Layout b) Embankment layout with DAS cable and sensor locations.

Table 1
Summary of index properties of Withy Beds clay.

Geotechnical property	Value
Liquid Limit (%)	56
Plastic Limit (%)	25
Plasticity Index (%)	31
Clay Fraction (d < 2 μm) (%)	41
Maximum Dry Unit Weight (kN/m^3)	17
Optimum Moisture Content (%)	24
Target Compaction Conditions	
Bulk Density (kg/m^3)	1800
Gravimetric Moisture Content	32

based on the procedures outlined in (*Geotechnical Investigation and Testing-Laboratory Testing of Soil-Part 12: Determination of Liquid and Plastic Limits*, 2018). Remoulded samples were prepared to a target gravimetric water content *w* of 32% to match that of block samples collected from site during the winter season, where suctions were close to zero. A target bulk density of 1800 kg/m^3 was used, which was selected based on density ring tests carried out *in-situ*. The *in-situ* void ratio of the soil, determined from density ring tests, was 0.94 (Table 1). The clay fraction in Table 1 was determined using the particle size distribution analysis (ASTM D7928–21) (ASTM D7928-21e1, 2021). The specimen was prepared in a standard proctor mould (Fig. 2a).

The compaction effort was adjusted to ensure that the initial void ratio of the laboratory specimen closely matched the *in-situ* condition (Hen-Jones et al., 2017). The prepared specimen had an initial diameter of 102 mm and height 116 mm. The specimen was then sealed and stored in an air-tight container for ensuring moisture equilibration for 24 h.

2.3. Specimen instrumentation

The soil specimen was instrumented with Teros (T-21) soil water potential sensor, manufactured by Meter Group. These sensor types were also installed in the embankment for *in-situ* matric suction measurements. The installation method, illustrated in Fig. 2 was followed to establish a solid connection between the sensor and the soil, minimising the risk of cavitation or air pockets that could potentially interfere with the sensor's readings. The soil specimen was encased in a series of 3D-printed acrylic moulds, designed to move independently, to hold the bender elements in contact to the soil during periods of volume change caused by shrinking and swelling (Fig. 2e and Fig. 2f).

2.4. Laboratory testing procedure

After the specimen was prepared, sealed and subjected to moisture homogenisation, it was allowed to dry at room temperature. It was subsequently subjected to three sets of drying and wetting (D/W) cycles, as illustrated in Fig. 3a. During the first drying phase, suction measurements were obtained at various moisture contents. These measurements were used to establish the Soil-Water Characteristic Curve (SWCC) for the Withy Beds clay (Fig. 3b). The weight and volume of the specimen was measured to monitor the change in its Volumetric Water Content VWC. Variations in specimen mass were used to determine moisture content at different suction levels. At each suction stage, the specimen diameter and height were measured using vernier callipers to quantify corresponding volume changes. By combining the moisture and volume change measurements at each suction level, the VWC was determined throughout this test. Based on the measurements obtained from the *in-situ* suction sensors, the embankment experienced a suction level of 1200 kPa during the summer period. To replicate these field conditions the specimen was dried to a moisture content of approximately 23%, to replicate the maximum *in-situ* matric suction. Once the specimen had dried sufficiently, it was rewetted to its approximate initial weight. The rewetting was performed by wrapping the specimen in a wet towel to ensure that its maximum surface area was exposed to the surrounding moisture.

During rewetting, the specimen was stored inside an airtight container to avoid loss of moisture. The weight, volume and suction of the specimen were monitored until the subsequent measurement point was reached.

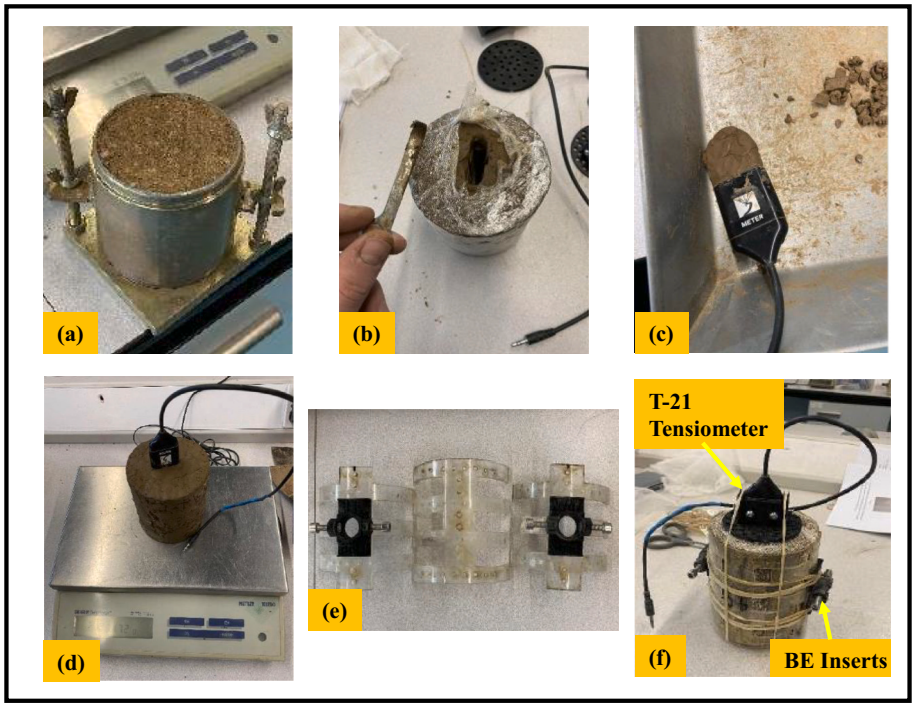

Fig. 2. Specimen preparation and instrumentation: a) Specimen prepared in standard proctor mould, b) Soil removed for placing the sensor, c) Sensor coated in the soil removed from the specimen, d) Sensor inserted into the specimen while ensuring proper connection between soil and sensor, e) 3-D printed acrylic casing, f) Specimen encased in 3-D printed acrylic casing.

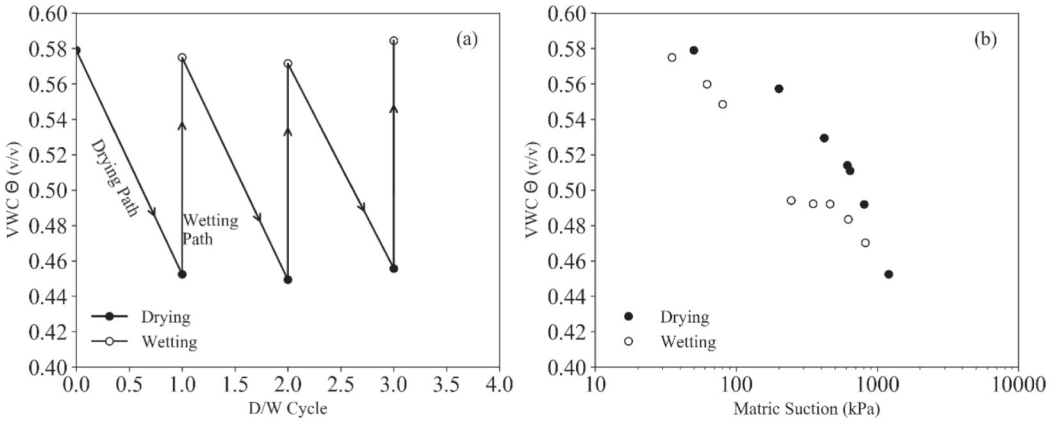

Fig. 3. a) Sequence of (D/W) cycles adapted in this study, b) SWCC for D/W cycle 1.

In Fig. 3b, the SWCC exhibits hysteresis as the moisture content at similar suction levels was lower during the wetting cycle in comparison to the drying cycle. Further discussion regarding this hysteretic behaviour will be provided in the results and discussion sections. To replicate the moisture variations experienced under *in-situ* conditions, this drying-wetting pathway was also applied to the specimen for the remaining cycles.

During each D/W cycle, V_s measurements were obtained at different points along the SWCC. Prior to each measurement, the specimen was sealed and stored in an airtight container for 24 h at the target moisture content to allow moisture equilibration. A 24 h equilibration period is sufficient for minimising moisture variation within the specimen for this type of study (Walker et al., 2023). The V_s signals were transmitted and received using a setup that included a Siglent function generator and a Picoscope 5000 series oscilloscope. A 10 V sine wave was used as the input signal. To account for the sample's changing stiffness during the drying and wetting phases, the input frequencies were adjusted. This ensured that the length-to-wavelength ratio (L_{tt}/λ) consistently exceeded the recommended value of 3 at each moisture level (Leong et al., 2005; Khan et al., 2019), thereby minimising near-field effects and enabling more accurate identification of S-wave arrival times (Bonal et al., 2012). V_s was determined from the travel distance between the tips of bender elements (L_{tt}) and the travel time was chosen as the time of first arrival (Δt) of the output shear wave signal: $V_s = (L_{tt}/\Delta t)$. This method is commonly adopted for determining shear wave travel time and has been widely used in previous studies investigating the influence of moisture variation on soil stiffness (Dong and Lu, 2016a; Walker et al., 2023; Yamashita et al., 2009; Mahmoodabadi and Bryson, 2021). The small-strain stiffness (G_0) was determined using the measured V_s and bulk density ρ of the specimen: $G_0 = \rho.(V_s)^2$.

It should be noted that no further suction measurements were obtained during D/W cycle 2 and 3 due to malfunction of the T-21 sensor at the end of cycle 1. Consequently, subsequent V_s measurements were limited to assessing the specimen's response to moisture variation across the remaining cycles.

2.5. Field instrumentation

The embankment is instrumented with soil moisture and matric suction sensors at 5 locations. These sensors were spaced 66 m apart, as shown in Fig. 1b. All sensors were buried at a depth of 0.5 m below the ground surface. Matric suction measurements of the soil are obtained using the T-21 sensor. The moisture is monitored using ECH_2O-5TE sensors (Meter Environment, formerly Decagon Devices, Inc., Pullman, WA, USA). These sensors are commonly termed as capacitance-based moisture sensors that can measure the VWC of the soil. The sensors require soil-specific calibration to obtain the correct moisture content as the factory calibration is generally not sufficiently accurate for all soil types (Lim et al., 2017; Kinzli et al., 2012). Following the manufacturer's recommended calibration procedure, the soil was mixed with water and placed in a 2 L container, with the sensor fully embedded to ensure complete contact with the wet soil. VWC was recorded and the calibration equation was obtained by relating the measured VWC to the known VWC of the soil. Eq. (1) was used in this study to obtain the calibrated field-based VWC measurements from the 5TE sensors:

$$\theta_{cal} = 1.67\theta_{raw} - 0.0084 \quad (1)$$

where, θ_{cal} is the calibrated VWC measurement and θ_{raw} is the original VWC measurement obtained from the field sensors.

2.6. DAS based data acquisition and processing

DAS data was acquired using a tight buffered cable that was buried in a shallow (approx. 10 cm deep) trench into the mid-slope of the embankment (Fig. 1b). An Optasense ODH4 interrogator unit was used for acquiring DAS data from the site, with a gauge length of 2 m and spatial sampling of 1 m. A sledgehammer was used as the source (Fig. 4a) for generating surface wave seismic waves.

To ensure precise and repeatable positioning of sources and receivers throughout the data collection period, permanent markers were installed along the survey area. As recommended by Donohue and Long (Donohue and Long, 2008), a number of different source- receiver array geometries were assessed in order to determine the optimum MASW acquisition parameters. Key parameters, including a 200 Hz sampling frequency, 1-m channel distance, and 15 m total receiver array length, were defined. In total, five active surveys are considered here (x = 34 m, x = 100 m, x = 166 m, x = 232 m, and x = 298 m), each centrally positioned over the field sensor locations, to provide a direct comparison with these data. Surveys were acquired on four separate occasions: 24 August 2022, 23 November 2022, 14 April 2023, and 23 August 2023.

Consistency in the data was ensured by using the same type of source, receiver, and recording equipment for each survey. The acquisition geometry and parameters were carefully maintained across all surveys to ensure the seismic data were fully comparable. Seismic data was processed using MASWaves (Olafsdottir et al., 2018), where dispersion images were generated for each seismic shot and dispersion curves were extracted using a minimum picking frequency of 5 Hz and a 95% confidence interval.

The subsequent inversion process involved estimating a single initial model, which was then applied for the deterministic inversion of surface wave data from the five locations. This approach is based on the methodology outlined by Bergamo et al. (Bergamo et al., 2011) and Boiero and Socco (Boiero and Socco, 2010). The initial model for inversion was obtained through Monte Carlo (MC) inversion of the

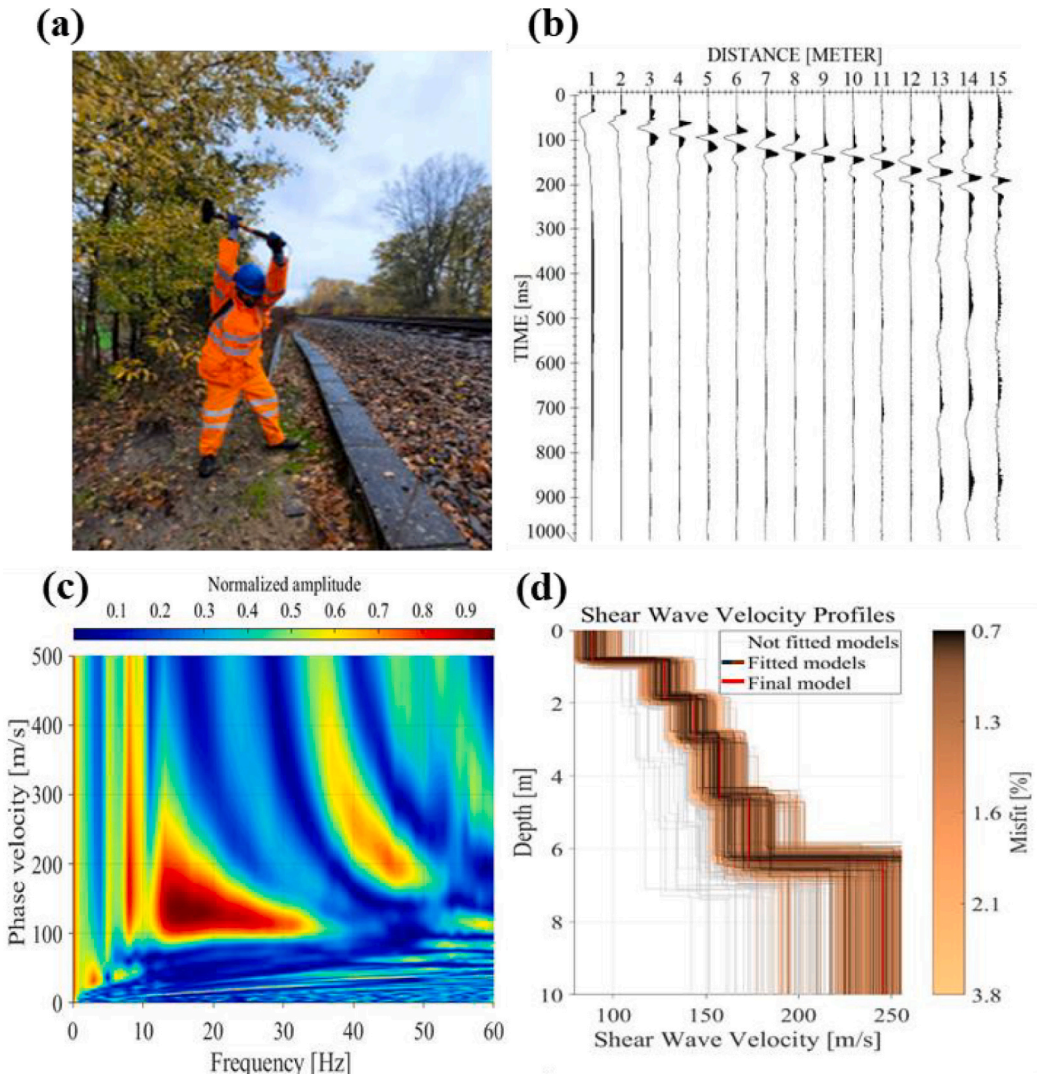

Fig. 4. Data Processing Workflow using the MASW method. a) Generation of seismic waves using a sledgehammer. b) A trimmed seismic section c) Rayleigh dispersion image d) Inverted V_s models with the final averaged best-fit model indicated by the red line. (For interpretation of the references to colour in this figure legend, the reader is referred to the web version of this article.)

sample dispersion curves. This involved selecting V_S models with different numbers of layers and thicknesses, specific to the site. After evaluating these models, a final V_S model, shown in Fig. 4d, was chosen to serve as the initial model for the inversion process. The MC inversion algorithm developed by Maraschini and Foti (Maraschini and Foti, 2010) was used in this study. This approach enables a computationally efficient search of the parameter space to be carried out. For each MC inversion, 104 models, with a fix number of layers (5), were tested. After the inversion, models with misfit values below 2 were considered optimal.

3. Results

3.1. Dependency of V_s and G_0 on matric suction

Due to their higher plasticity, clayey soils generally exhibits hysteresis when subjected to drying and wetting (Gapak and Tadikonda, 2018; Lu and Khorshidi, 2015). Similar behaviour is also observed in the SWCC obtained for the Withy Beds clay (Fig. 3b). Therefore, obtaining V_s measurements helps provide insight into the shear stiffness behaviour of the clay along the drying and wetting parts of the SWCC (Dong and Lu, 2016a; Dong and Lu, 2016b; Walker et al., 2023; Mahmoodabadi and Bryson, 2021; Irfan et al., 2024). The shear wave traces for the first D/W cycle are illustrated in Fig. 5a. Each trace is also accompanied by the L_{tt}/λ value measured using the input frequency required to generate the shear wave signal. Suction data was only collected for first D/W cycle (Fig. 5a). As shown for each D/W cycle, the V_s increased during drying from an initial suction of 50 kPa ($w = 0.32$), to 1200 kPa ($w = 0.23$). Upon rewetting, the V_s reduced as the specimen softened due to the absorption of water.

A plot of V_s with suction is shown in Fig. 6a. During drying, a lower rate of increase in V_s is observed between suctions of 50 kPa and 200 kPa, with values rising from approximately 115 m/s at 50 kPa to 125 m/s. Beyond 500 kPa, V_s increases more rapidly to 150 m/s. With further drying, V_s continues to increase and exceeds 200 m/s at 1200 kPa. The corresponding trend in G_0, with respect to suction, is shown in Fig. 6b, where the stiffness increases from 23 MPa in the initial state to 40 MPa at a matric suction of about 500 kPa. Beyond this point, G_o increases more rapidly, more than doubling as matric suction exceeds 500 kPa and reaching approximately 85 MPa at 1200 kPa.

During the subsequent wetting cycle, the values of V_s and G_0 are higher than their corresponding values during the drying cycle at similar suction values, indicating the presence of hysteresis in the stiffness-suction relationship. Further suction-moisture measurements were not

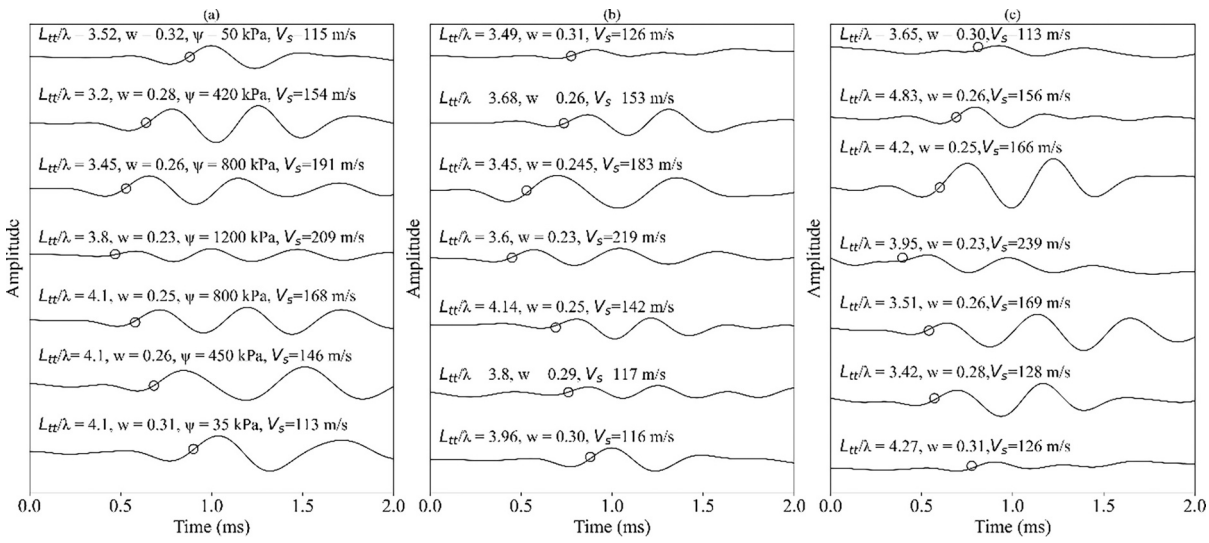

Fig. 5. Shear wave trace evolution across D/W cycles: a) D/W Cycle 1, b) D/W Cycle 2, c) D/W Cycle 3. Note: Each trace is accompanied by L_{tt}/λ ratio, gravimetric moisture content w matric suction ψ and V_s.
Note: The circle represents the chosen time of first arrival on each trace.

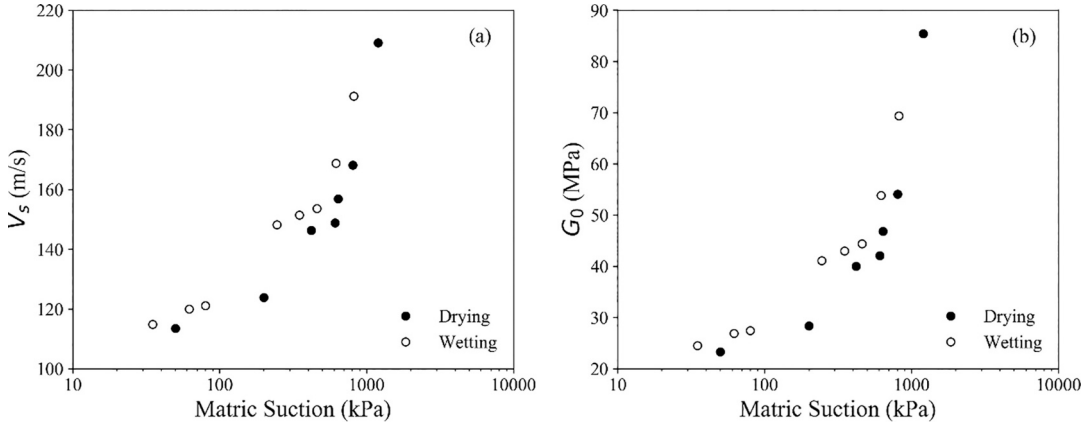

Fig. 6. a) V_s *vs* matric suction for D/W Cycle 1, b) G_0 *vs* matric suction for D/W Cycle 1.

obtained in subsequent cycles due to malfunction of the T-21 sensor at the end of the first D/W cycle. The study therefore proceeded by monitoring the influence of moisture variation on V_s during the remaining D/W cycles.

3.2. Dependency of V_s and G_0 on water content

Shear wave traces for all-three D/W cycles are provided in Fig. 5. The dependency of V_s on moisture content in each of the three cycles is illustrated in Fig. 7a, b and c. For the first D/W cycle, the hysteresis observed in the specimen's V_s with suction (Fig. 6a), is not as obvious in Fig. 7a. During rewetting, *Vs* values are generally similar to, or slightly lower than, those recorded along the drying path. However, the specimen exhibits clear dependency of V_s on varying moisture levels during each of the three D/W cycles. The specimen exhibited pronounced hysteresis in the second D/W cycle as higher V_s values were observed during the wetting phase. However, the hysteresis becomes less evident in cycle 3.

The variation in G_0 with VWC is shown in Fig. 7d, e and f, together with power-law fits for each cycle, consistent with relationships reported by (Dong and Lu, 2016a; Lu and Kaya, 2014). During the drying phase of each D/W cycle, the power law exponents indicate increasingly stiffer behaviour. With successive cycles, the rate of stiffness increase during drying becomes more pronounced, as reflected by the exponent rising from 5.22 in cycle 1 to 5.82 in cycle 3. A similar trend is observed during the wetting phases, where the exponent increases from 5.03 in cycle 1 to 5.40 in cycle 3. This illustrates that the drop in stiffness with increasing moisture during wetting is steadily occurring at a higher rate across the D/W cycles.

3.3. Dependency of G_0 on volumetric strain

Fig. 8 illustrates the relationship between G_0 and volumetric strain for all D/W cycles. Volumetric strain was calculated from the change in specimen volume relative to its initial prepared state.

During the drying stage of each D/W cycle, difference in G_0 between cycles are most pronounced at lower strain values. The shear stiffness of the specimen drying the first D/W cycle is higher than the stiffness in the remaining two cycles at volumetric strains below 0.1. However, at volumetric strain exceeding 0.1, a steeper increase in stiffness is observed during D/W cycles 2 and 3. Upon rewetting, the reduction in stiffness with volumetric strain is similar across all three cycles. As the specimen swells by absorbing moisture, the stiffness in each wetting cycle converges at strains below 0.1.

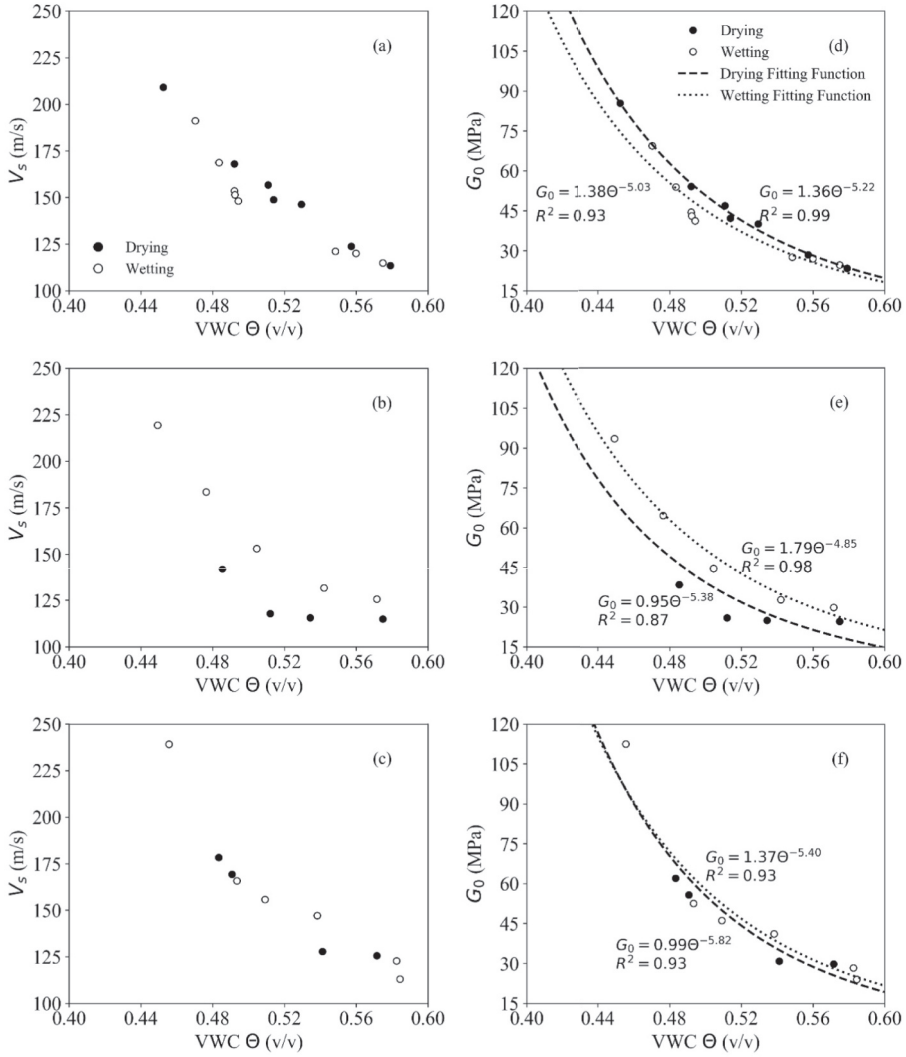

Fig. 7. Dependency of V_s and G_0 on VWC: a) V_s in D/W Cycle 1, b) V_s in D/W Cycle 2, c) V_s in D/W Cycle 3, d) G_0 in D/W Cycle 1, e) G_0 in D/W Cycle 2, f) G_0 in D/W Cycle 3.

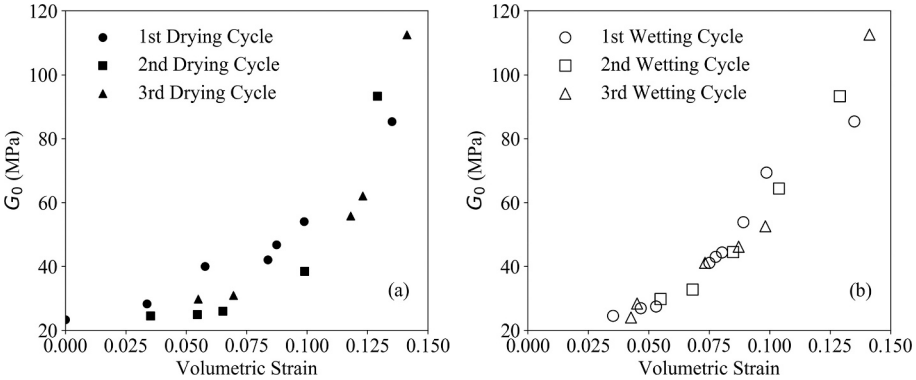

Fig. 8. a) G_0 *vs* volumetric strain in each drying cycle b) G_0 *vs* volumetric strain in each wetting cycle.

3.4. Field sensor results

In Fig. 9, the measurements from suction and VWC sensors located at 5 points along the embankment are illustrated. These measurements were obtained from August 2022 to August 2023, as this covers the period within which the active seismic surveys were performed. VWC measurements obtained from the sensors were corrected using Eq. 1. The soil temperature profile over the testing period, shown in Fig. 9b, represents the monthly averaged measurements from all 5TE sensors.

The soil moisture deficit (SMD) is also shown in Fig. 9a. SMD represents the volume of water required per unit area of soil to return it to field capacity and is expressed in millimetres (mm). Field capacity refers to the equilibrium moisture condition at which excess water drains freely under gravity. As such, SMD provides an indication of the degree

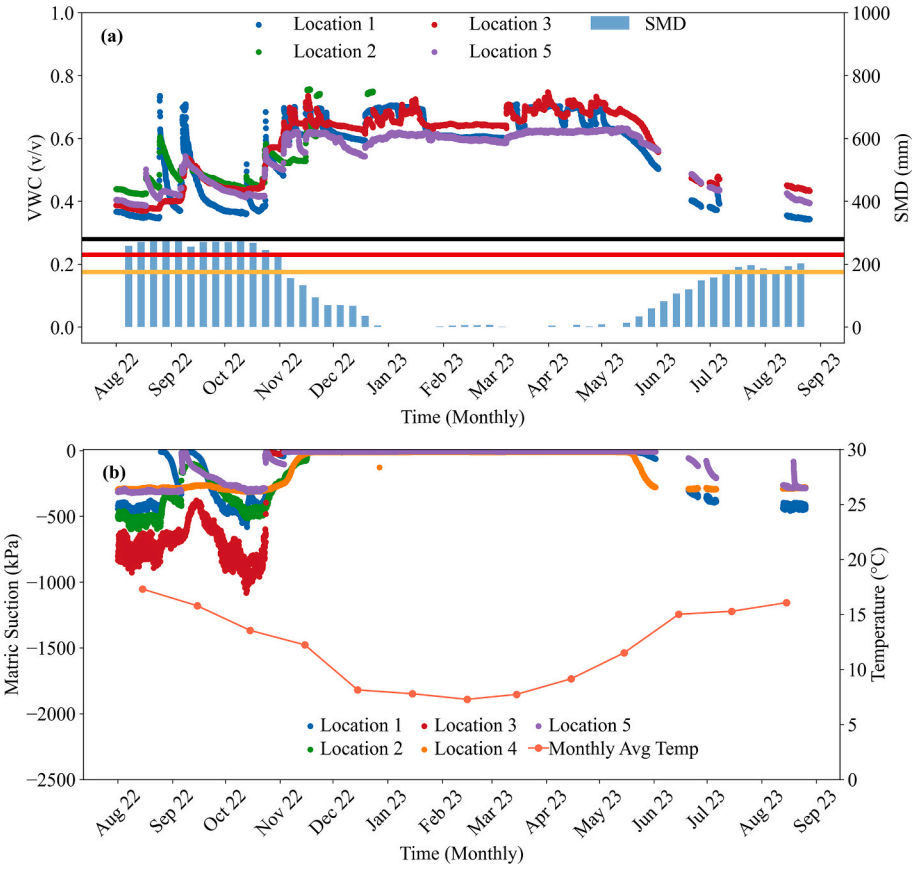

Fig. 9. Sensor data between Aug-22 and Aug-23, a) Hourly VWC measurements and weekly SMD data from MORECS (Irfan et al., 2024) together with Network Rail thresholds (amber, red, black), b) Hourly matric suction measurements and averaged monthly temperature measurements of soil at 0.5 m depth.
Note: The bars illustrate the range between the maximum and minimum average temperature recorded by all the sensors during the month. (For interpretation of the references to colour in this figure legend, the reader is referred to the web version of this article.)

of soil drying and available storage for incoming rainfall. By correlating SMD and reported slope failures in London clay, Ridley et al. (Ridley et al., 2004) demonstrated the significance of SMD for monitoring embankment stability. The SMD data plotted in Fig. 9a is generated weekly by UK met office using MORECS (Meteorological Office Rainfall and Evaporation Calculation System) (Hough et al., 1997).

In August 2022, VWC across the embankment consistently varies between 35% and 45% *v*/v, as shown by sensors 1, 2, 3 and 5. VWC measurements from location 4 are not included in the analysis as the VWC sensor malfunctioned at this location. Across all sensors, the moisture levels remain below 50% up to early November. Although the SMD data are not site-specific, values exceeding 200 mm indicate notably dry ground conditions during these periods. The suction measurements in this period exceed 250 kPa in all sensors (Fig. 9b), with the sensor at location 3 recording suctions greater than 1000 kPa. The onset of wetter conditions in December is characterised by increasing VWC and a corresponding reduction in matric suction. During the winter period, lower ground temperatures (below 10 °C) reduce evapotranspiration and promote moisture retention within the embankment, resulting in elevated VWC, typically ranging between 60% v/v and 75% v/v, and consistently low matric suction across the slope. The lower rate of evapotranspiration in the period between December 2022 and May 2023 is also characterised by SMD values remaining close to zero throughout these months. In late Spring, early summer of 2023, as the temperature and evapotranspiration rates begin to rise, the VWC readings drop below 60% v/v. The suction also reaches up to 500 kPa in late June 2023 at location 1 while the SMD begins to increase in June, reaching up to 200 mm during August. During this summer, the VWC stabilises between 35% v/v and 45% v/v in August 2023. Although both sensors at location 2 stopped recording any further measurements in late 2022, the rest of the moisture measurements exhibited similar trends across 2023. Furthermore, the suction sensor at location 3 also did not record in 2023.

However, a similar range of moisture and suction measurements was recorded by the rest of the sensors. These measurements were in close agreement to those observed in August 2022 at locations 1,4 and 5. The soil sensor measurements illustrate the variation in the embankment to the changing moisture throughout the year.

3.5. *Inverted S-Wave Velocity from DAS based MASW surveys*

The inverted V_s profiles from each of the five locations are shown in Fig. 10. At most locations, the dry conditions observed in August 2022 and 2023 resulted in elevated V_s values within the near-surface zone, extending to approximately 2 m depth. At this depth, the V_s values exceed 160 m/s in locations 1 and 2. The V_s values decline in November, dropping below 125 m/s at approximately 2 m depth in locations 2 and 3.

Based on the laboratory-based measurements in Fig. 6a and Fig. 7, V_s values below 125 m/s represent high moisture conditions (VWC > 60% *v*/v) where the soil has low matric suction (< 50 kPa). During the winter and early months of spring 2023, the embankment experienced further wet conditions, as demonstrated by the low suction and SMD between January and May 2023. As a result, a further loss of stiffness occurred as the V_s fell below values observed in November 2022.

During the summer of 2023, an increase in evapotranspiration rates, marked by higher soil temperature and increasing SMD, resulted in a corresponding increase in matric suction, enabling the embankment to

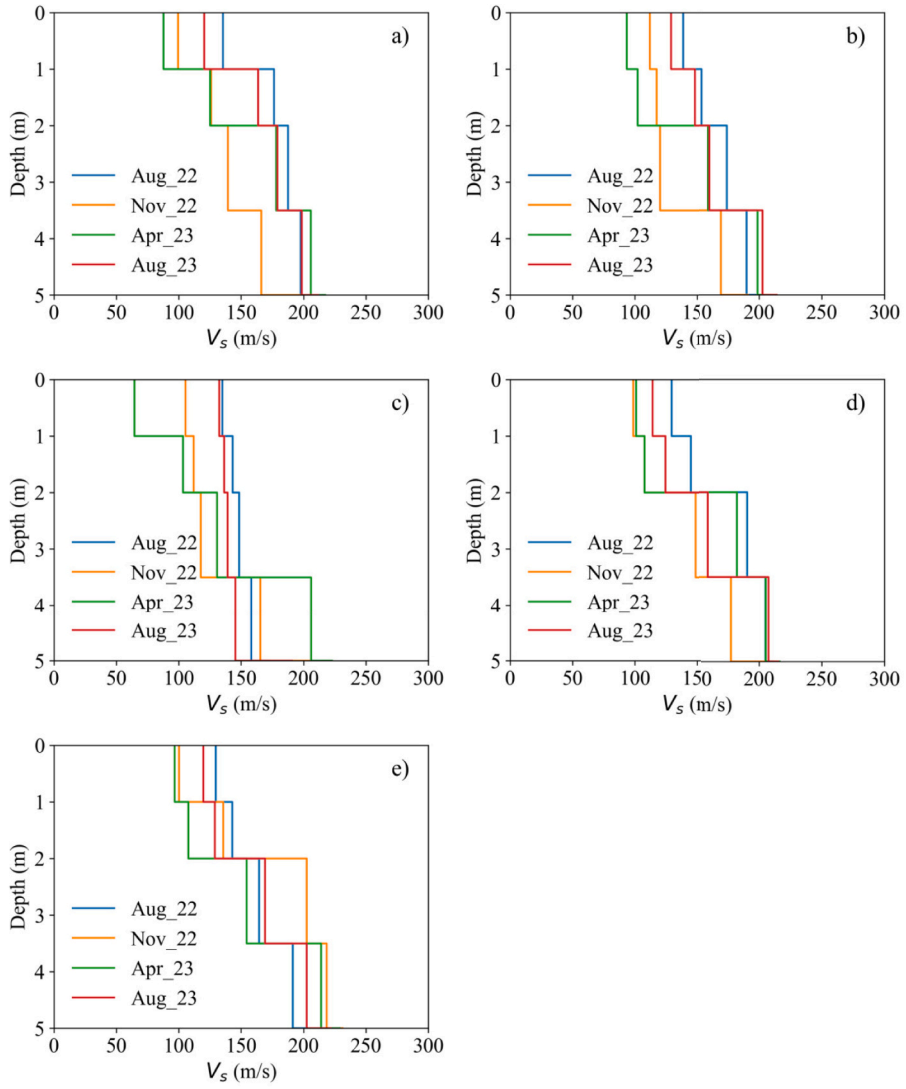

Fig. 10. Inversion results from MASW survey, a) Location 1 b) Location 2 c) Location 3 d) Location 4 e) Location 5.

regain stiffness. This is demonstrated the by higher V_s values in August 2023.

In Fig. 9a, the SMD thresholds adopted by Network Rail to indicate serviceability risks under very dry conditions are shown: amber at 175 mm, red at 230 mm, and black at 280 mm. With the embankment experiencing low moisture and high suction in August 2022, SMD values between the red and black thresholds correspond to V_s values exceeding 150 m/s at locations 1 and 2. In contrast, the milder drying conditions in August 2023 resulted in SMD values below the red threshold, with the corresponding V_s values at each location remaining lower than those recorded in the previous year. The correlation between SMD, sensor data, and V_s observed during summer highlights that when V_s exceeds approximately 150 m/s, the embankment is likely to experience increased serviceability concerns requiring intervention by Network Rail.

4. Discussion

The embankment response to seasonal moisture variations was monitored using sensors and geophysical methods. V_s measurements consistently captured the moisture dependency of the Withy Beds embankment throughout the monitoring period. To support interpretation of these field observations, laboratory testing was undertaken to develop a clearer understanding of the geophysical and volumetric behaviour of Withy Beds (London) clay under controlled moisture variations.

In Fig. 11, the variation of G_0 at end of wetting and drying phases across each cycle is shown. The specimen showed a progressive increase in stiffness at the end of each drying phase, whereas no comparable

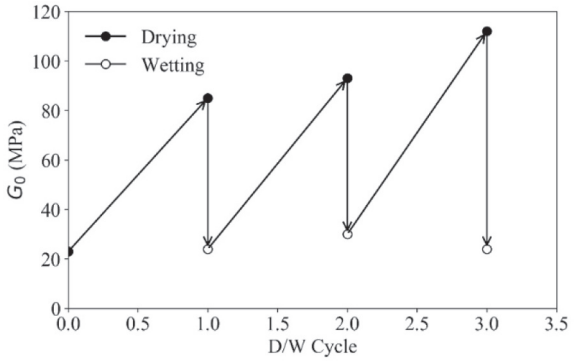

Fig. 11. Variation of G_0 during at end of wetting and drying across all D/W cycles.

increase was observed following wetting phases. The increase in stiffness exhibited by the specimen during each drying phase was previously observed for kaolin clay (Walker et al., 2023). Consistent with the present findings, the kaolin specimen did not demonstrate a pronounced rise in stiffness at the end of the wetting phase. Dong and Lu (Dong and Lu, 2016b) demonstrated that, in the absence of externally applied stresses, variations in G_o are primarily governed by capillary water, which influences suction stress through changes in inter-particle contact stresses. The concept of suction stress, as outlined by Lu (Lu and Likos, 2006), provides a framework linking matric suction to interparticle forces *via* the SWCC. As suction stress governs stiffness within the capillary regime, G_o increases during drying. Below 200 kPa, where moisture content remains above the air-entry value, only a modest increase in G_o is observed (Fig. 7d–f); once moisture falls below the air-entry point, G_o rises more significantly. During wetting, adsorption of water reduces suction stresses between soil particles, causing the specimen to approach saturation and resulting in a decrease in G_o.

Earlier studies have shown that hysteresis in soils is linked to soil plasticity (Gapak and Tadikonda, 2018; Lu and Khorshidi, 2015). With 41% clay fraction and higher values of PI and LL, the highly plastic nature of London clay used in the current study is likely to exhibit hysteretic behaviour. The difference in moisture content at the same suction level is likely due to the varying volumetric response of entrapped air during drying and wetting. Furthermore, the difference in response of water menisci on the soil-water interfaces during drying and wetting also cause hysteresis in the SWCC and G_0-matric suction relationship. These variations in moisture response to wetting and drying results in a pore structure that causes the specimen to have a stiffer response to wetting. Similar results for various soil types have also been observed in earlier studies (Walker et al., 2023; Khosravi et al., 2016; Khosravi et al., 2020). During the initial D/W cycle, the size of hysteresis loop is typically larger for remoulded soils compared to natural soils (Mu et al., 2020). This is attributed to the ink-bottle effect, entrapped air and contact angle effects prevalent in the soil matrix due to the irregular size and shape of individual and interconnected pores (Goh et al., 2015; Zhang et al., 2020; Hillel, 2013; Masrouri et al., 2008). Upon further D/W cycles, the size of the hysteresis loop decreases as the internal soil structure stabilises (Mu et al., 2020; Xu et al., 2020). The dominant minerology of London clay typically comprises illite-smectite mix and kaolinite (Monroy et al., 2010; Kemp and Wagner, 2006). While highly plastic clays such as London clay would exhibit hysteresis, soils dominated by montmorillonite generally exhibit more pronounced hysteresis than those with an illite–smectite mix and kaolinite (Lu and Khorshidi, 2015; Xu et al., 2020). The soil mineralogy and stabilisation of internal pore structure might have revealed reduced hysteresis along the wetting and drying paths but the absence of concurrent suction measurements with V_s limits the strength of such an interpretation.

Fig. 12 illustrates the relationship between field- and laboratory-based V_s values. The sensor measurements represent the average of VWC (and matric suction) values recorded by the sensors on the day of the active geophysical survey. The V_s values are taken as average at approximately 2 m depth from the inverted field profiles (Fig. 10). This depth corresponds to the near-surface zone where V_s shows consistent seasonal variation across all locations.

Although field-based V_s values fall somewhat outside the range obtained in the laboratory, both datasets exhibit consistent moisture-dependent behaviour. Differences between field and laboratory V_s values are attributed to differences in soil fabric and stress state. The embankment, originally constructed from locally end-tipped clays, has undergone decades of drying–wetting cycles that have modified its pore structure and moisture retention characteristics (Stirling et al., 2021). At higher moisture contents, the laboratory-based power-function fit tends to underestimate field V_s values, likely due to the influence of *in-situ* overburden stresses on embankment stiffness. In contrast to the V_s-moisture relationship, the field V_s-suction relationship shows closer agreement with the laboratory results, despite some variability in the data. This observation is consistent with previous studies that highlight the dominant role of soil suction in governing stiffness behaviour in fine-grained soils. Furthermore, it establishes suction monitoring as a useful indicator for assessing embankment condition under seasonal moisture variations. Some scatter between laboratory and field datasets is also expected due to differences in measurement scale. Bender element tests represent element-scale behaviour within a small, localised soil volume, whereas MASW-derived V_s values provide an averaged response over a larger subsurface volume. Overall, it appears that accurate interpretation of *in-situ* geophysical data requires site-specific moisture and suction relationships, further work is required to confirm this.

While the relationships established between *in-situ* and laboratory-based V_s measurements, together with moisture and suction data, provide valuable insight into soil behaviour, the study is limited to a single clay embankment site. Although many historic embankments in the UK are constructed from high-plasticity clays, differences in mineralogy may lead to varying responses to seasonal moisture change, and further investigation at comparable sites is required to extend the applicability of the approach. Differences in the rate of moisture change between field and laboratory conditions, together with the use of remoulded specimens, mean that long-term ageing and relaxation effects inherent to *in-situ* embankments are not fully captured. Additional studies employing suction-controlled, rather than moisture-controlled, laboratory testing would provide further insight into the dependence of V_s on the stress state within the soil matrix. Finally, although long-term railway loading may influence near-surface ground conditions, particularly within ballast layers, the stiffness variations observed in this study are interpreted to be primarily controlled by moisture-driven hydro-mechanical

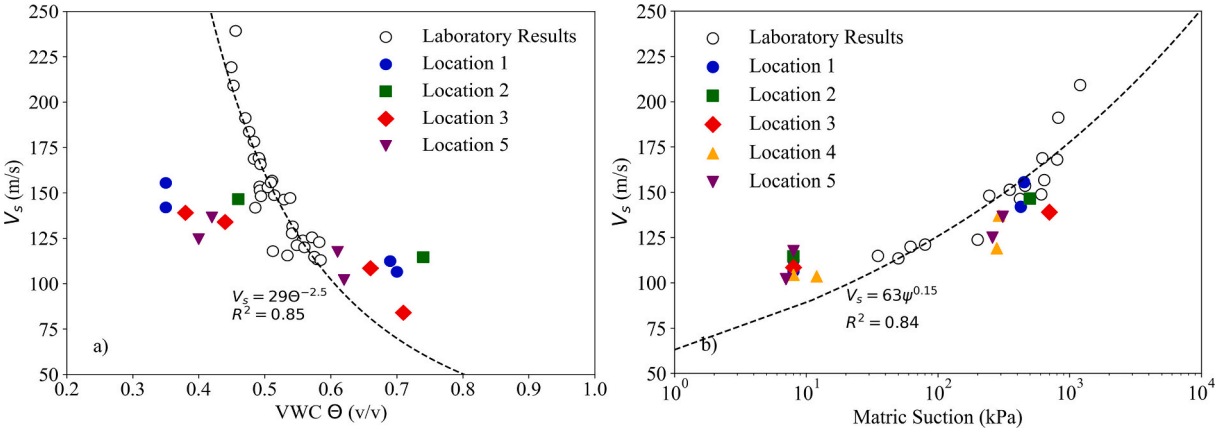

Fig. 12. Inter-relationship between MASW and laboratory-based V_s measurements using soil sensor data a) V_s v VWC b) V_s v Matric Suction.

processes within the clay embankment fill.

Despite these limitations, the study demonstrates the potential of an integrated field-laboratory investigation framework to support the critical assessment of historic embankments, particularly in understanding their performance limits under extreme climatic conditions. In addition, this study has used active sledgehammer seismic surveying as a means of determining field V_s, this approach is somewhat unsuitable for longer term temporal monitoring. Recent work, has, however, indicated the potential benefits of using DAS for time-lapse monitoring of passive seismic noise, enabling the continuous measurement of V_s with high spatial and temporal resolution (Trafford et al., 2024b). Also, based on the laboratory findings, high V_s values may indicate the potential for volume change, including possible shrinkage induced cracking, due to the non-linear rate of increase in stiffness at higher volumetric strain levels (Fig. 8). The use of these measurements could, therefore, support the case for possible engineering interventions, for example associated with the imposition of speed restrictions on railways. Although, as discussed previously; to improve the utility of such interventions, site specific moisture, V_s and matric suction relationships are critical in the application of geophysical monitoring.

5. Conclusions

This study presents a combined field and laboratory investigation of the moisture-dependent behaviour of a clay-rich railway embankment fill. MASW monitoring was used to assess the response of an instrumented embankment over a 12-month period. Laboratory testing characterised the SWCC and V_s response across three D/W cycles.

Four active MASW surveys conducted between August 2022 and September 2023 demonstrated a clear dependency of *in-situ* V_s on seasonal moisture variation. During the dry summer months, characterised by high matric suction, elevated temperature, and high SMD, V_s values exceeded 140 m/s at locations 1 and 2, corresponding to SMD levels between the red (230 mm) and black (280 mm) thresholds adopted by Network Rail. In contrast, the milder summer of 2023, with SMD below the red threshold, showed lower V_s values. During the wetter winter months, V_s values dropped below 110 m/s under low suction and high moisture conditions, indicating softer embankment conditions. These findings suggest that V_s values exceeding approximately 140 m/s can serve as an indicator of potential serviceability concerns, providing a quantifiable link between soil stiffness, SMD, and embankment performance. Although this study focuses on stiffness characterisation and monitoring in clay-rich embankments, the spatial and temporal information provided by DAS-based MASW has clear potential to inform the targeting, timing, and evaluation of engineering interventions for other geotechnical works. Repeatable V_s measurements could be used to support the assessment of ground improvement and stabilisation strategies (Yesnik et al., 2025; Li et al., 2018; Saneiyan et al., 2018). Such monitoring approaches are particularly relevant for binder stabilisation aimed at improving the performance of collapsible soils (Asadoullahtabar et al., 2024) and clays (Lindh and Lemenkova, 2022; Subramanian et al., 2020).

V_s measurements were also obtained for specimens prepared in the laboratory using bender elements. These specimens were subjected to the range of suction and moisture levels that the embankment experienced during the monitoring period. By subjecting the specimen to multiple D/W cycles, the stiffness (G_0) response of the embankment clay to moisture variation was examined. The highly plastic nature of London clay resulted in pronounced hysteresis during the first drying–wetting (D/W) cycle, with G_0 values during wetting generally higher than those at similar suction levels during drying. This hysteresis would be expected to reduce with additional suction cycles; however, further cycles were not performed in this study. Furthermore, the specimen exhibited progressively stiffer behaviour with additional drying cycles, as indicated by increasing G_0 measurements at the end of each drying cycle.

Although field V_s values at similar moisture levels were outside the laboratory range, both datasets showed consistent moisture dependency. A stronger correlation of V_s with matric suction indicates that suction is a more reliable parameter for assessing stiffness. Therefore, characterising vulnerable embankments using field and laboratory geophysical studies have considerable potential in understanding the response of these structures to moisture variation.

CRediT authorship contribution statement

Qasim Khan: Writing – review & editing, Writing – original draft, Visualization, Validation, Resources, Methodology, Investigation, Conceptualization. **Muhammad Saqlain:** Writing – review & editing, Software, Methodology, Investigation, Formal analysis, Data curation, Conceptualization. **Andrew Trafford:** Visualization, Resources, Investigation. **Ben Dashwood:** Resources, Methodology, Investigation. **J.E. Chambers:** Resources, Methodology, Investigation. **Gavin Jessamy:** Supervision, Resources, Project administration, Methodology. **Julian Harms:** Supervision, Resources, Project administration, Methodology. **Shane Donohue:** Writing – review & editing, Visualization, Validation, Supervision, Project administration, Investigation, Funding acquisition.

Declaration of competing interest

The authors declare that they have no known competing financial interests or personal relationships that could have appeared to influence the work reported in this paper.

Acknowledgement

The research described in this paper has been funded with the financial support of Research Ireland, Geological Survey of Ireland and the Environmental Protection Agency under the Frontiers for the Future Programme grant 19/FFP/6535. The second author also acknowledges iCRAG - the Research Ireland Centre in Applied Geosciences, for their funding, (iCRAG-Phase 2 – Grant Code: 13/RC/2092_P2). Ben Dashwood and Jonathan Chambers publish with the permission of the Executive Director, British Geological Survey (UKRI-NERC).

Data availability

The measurement data is available from the corresponding author by request.

References

Asadoullahtabar, S.R., Asgari, A., Tabari, M.M.R., 2024. Assessment, identifying, and presenting a plan for the stabilization of loessic soils exposed to scouring in the path of gas pipelines, case study: Maraveh-Tappeh city. Eng. Geol. 342, 107747.

ASTM D7928-21e1, 2021. Standard Test Method for Particle-Size Distribution (Gradation) of FineGrained Soils Using the Sedimentation(Hydrometer) Analysis. American Society for Testing Materials, West Conshohocken, PA.

Bergamo, P., Comina, C., Foti, S., Maraschini, M., 2011. Seismic characterization of shallow bedrock sites with multimodal Monte Carlo inversion of surface wave data. Soil Dyn. Earthq. Eng. 31 (3), 530–534.

Bergamo, P., Dashwood, B., Uhlemann, S., Swift, R., Chambers, J.E., Gunn, D.A., Donohue, S., 2016a. Time-lapse monitoring of climate effects on earthworks using surface waves. Geophysics 81 (2), EN1–EN15.

Bergamo, P., Dashwood, B., Uhlemann, S., Swift, R., Chambers, J.E., Gunn, D.A., Donohue, S., 2016b. Time-lapse monitoring of fluid-induced geophysical property variations within an unstable earthwork using P-wave refraction. Geophysics 81 (4), EN17–EN27.

Biddle, G., 2001. Tree root damage to buildings. In: Expansive clay soils and vegetative influence on shallow foundations, pp. 1–23.

Boiero, D., Socco, L.V., 2010. Retrieving lateral variations from surface wave dispersion curves. Geophys. Prospect. 58 (6), 977–996.

Bonal, J., Donohue, S., McNally, C., 2012. Wavelet analysis of bender element signals. Géotechnique 62 (3), 243–252.

Briggs, K.M., Loveridge, F., Glendinning, S., 2017. Failures in transport infrastructure embankments. Eng. Geol. 219, 107–117.

Cho, G.C., Santamarina, J.C., 2001. Unsaturated particulate materials — particle-level studies. J. Geotech. Geoenviron. Eng. 127 (1), 84–96.

Clarke, D., Smethurst, J., 2010. Effects of Climate Change on Cycles of Wetting and Drying in Engineered Clay Slopes in England. Geological Society of London.
Coughlan, M., Trafford, A., Corrales, S., Donohue, S., Wheeler, A.J., Long, M., 2023. Geological and geotechnical characterisation of soft Holocene marine sediments: a case study from the north Irish Sea. Eng. Geol. 313, 106980.
Dong, Y., Lu, N., 2016a. Dependencies of shear wave velocity and shear modulus of soil on saturation. J. Eng. Mech. 142 (11), 04016083.
Dong, Y., Lu, N., 2016b. Correlation between small-strain shear modulus and suction stress in capillary regime under zero total stress conditions. J. Geotech. Geoenviron. Eng. 142 (11), 04016056.
Dong, Y., Lu, N., McCartney, J.S., 2016. Unified model for small-strain shear modulus of variably saturated soil. J. Geotech. Geoenviron. Eng. 142 (9), 04016039.
Donohue, S., Long, M., 2008. Assessment of an MASW technique incorporating discrete particle modelling. J. Environ. Eng. Geophys. 13 (2), 57–68.
Donohue, S., Long, M., 2010. Assessment of sample quality in soft clay using shear wave velocity and suction measurements. Géotechnique 60 (11), 883–889.
Donohue, S., Trafford, A., Gunn, D., Dashwood, B., Swift, R., McKillen, D., Leemon, D., 2019. Assessment of reservoir embankment dam condition using field and laboratory geophysical techniques. In: 1st Conference on Geophysics for Infrastructure Planning Monitoring and BIM, 2019. European Association of Geoscientists & Engineers, pp. 1–5 no. 1.
Driscoll, R., 1983. The influence of vegetation on the swelling and shrinking of clay soils in Britain. Geotechnique 33 (2), 93–105.
Fernández Ruiz, M.d.R., Soto, M.A., Williams, E., Martín López, S., Zhan, Z., González Herráez, M., Fidalgo Martins, H., 2020. Perspective on Distributed Acoustic Sensing for Seismic Activity Monitoring.
Fredlund, D.G., 2019. State of practice for use of the soil-water characteristic curve (SWCC) in geotechnical engineering. Can. Geotech. J. 56 (8), 1059–1069.
Fredlund, D.G., Xing, A., 1994. Equations for the soil-water characteristic curve. Can. Geotech. J. 31 (4), 521–532.
Fredlund, D.G., Sheng, D., Zhao, J., 2011. Estimation of soil suction from the soil-water characteristic curve. Can. Geotech. J. 48 (2), 186–198.
Gapak, Y., Tadikonda, V.B., 2018. Hysteretic water-retention behavior of bentonites. J. Hazard. Toxic Radioactive Waste 22 (3), 04018008.
Geotechnical Investigation and Testing-Laboratory Testing of Soil-Part 12: Determination of Liquid and Plastic Limits, 2018.
Goh, S., Rahardjo, H., Leong, E., 2015. Modification of triaxial apparatus for permeability measurement of unsaturated soils. Soils Found. 55 (1), 63–73.
Gunn, D., Dashwood, B.A., Bergamo, P., Donohue, S., 2016. Aged embankment imaging and assessment using surface waves. Proc. Inst. Civil Eng. Forens. Eng. 169 (4), 149–165.
Gunn, D., Chambers, J., Dashwood, B., Lacinska, A., Dijkstra, T., Uhlemann, S., Swift, R., Kirkham, M., Milodowski, A., Wragg, J., 2018. Deterioration model and condition monitoring of aged railway embankment using non-invasive geophysics. Constr. Build. Mater. 170, 668–678.
Hen-Jones, R., Hughes, P., Stirling, R., Glendinning, S., Chambers, J., Gunn, D., Cui, Y., 2017. Seasonal effects on geophysical–geotechnical relationships and their implications for electrical resistivity tomography monitoring of slopes. Acta Geotech. 12, 1159–1173.
Hillel, D., 2013. Fundamentals of Soil Physics. Academic Press.
Holmes, J., Chambers, J., Wilkinson, P., Dashwood, B., Gunn, D., Cimpoiaşu, M., Kirkham, M., Uhlemann, S., Meldrum, P., Kuras, O., 2022. 4D electrical resistivity tomography for assessing the influence of vegetation and subsurface moisture on railway cutting condition. Eng. Geol. 307, 106790.
Hough, M., Palmer, S., Weir, A., Barrie, I., 1997. The Meteorological Office Rainfall and Evaporation Calculation System: MORECS Version 2.0.
Hulme, M., 2002. Climate Change Scenarios for the United Kingdom: The UKCIP02 Scientific Report. Tyndall Centre for Climate Mental Sciences University.
Irfan, M., Rasool, A.M., Aziz, M., Ali, U., Niazi, F., Uchimura, T., 2024. Development of wetting-drying curves from elastic wave velocities using a novel triaxial test apparatus. Stud. Geotechn. Mechan. 46, 111–124.
Kang, J., Walter, F., Halter, T., Paitz, P., Fichtner, A., 2025. Soil slope monitoring with distributed acoustic sensing under wetting and drying cycles. Earth Surf. Dyn. 13 (6), 1133–1155.
Kemp, S., Wagner, D., 2006. The Mineralogy, Geochemistry and Surface Area of Mudrocks from the London Clay Formation of Southern England.
Khan, Q., Subramanian, S., Wong, D.Y., Ku, T., 2019. Bender elements in stiff cemented clay: shear wave velocity correction by applying wavelength considerations. Can. Geotech. J. 56 (7), 1034–1041.
Khosravi, A., Salam, S., McCartney, J.S., Dadashi, A., 2016. Suction-induced hardening effects on the shear modulus of unsaturated silt. Int. J. Geomechan. 16 (6), D4016007.
Khosravi, A., Hashemi, A., Ghadirianniari, S., Khosravi, M., 2020. Variation of small-strain shear modulus of unsaturated silt under successive cycles of drying and wetting. J. Geotech. Geoenviron. Eng. 146 (7), 04020050.
Kinzli, K.-D., Manana, N., Oad, R., 2012. Comparison of laboratory and field calibration of a soil-moisture capacitance probe for various soils. J. Irrig. Drain. Eng. 138 (4), 310–321.
Leong, E.C., Yeo, S.H., Rahardjo, H., 2005. Measuring shear wave velocity using bender elements. Geotech. Test. J. 28 (5), 488–498.
Li, C., Ashlock, J.C., Lin, S., Vennapusa, P.K., 2018. In situ modulus reduction characteristics of stabilized pavement foundations by multichannel analysis of surface waves and falling weight deflectometer tests. Constr. Build. Mater. 188, 809–819.
Lim, S., Shin, M., Son, J., Song, J., Cho, K., Lee, S., Ryu, J.-H., Cho, J.Y., 2017. Evaluation of soil pore-water salinity using a Decagon GS3 sensor in saline-alkali reclaimed tidal lands. Comput. Electron. Agric. 132, 49–55.
Lindh, P., Lemenkova, P., 2022. Shear bond and compressive strength of clay stabilised with lime/cement jet grouting and deep mixing: a case of Norvik, Nynäshamn. Nonlinear Eng. 11 (1), 693–710.
Lu, N., Kaya, M., 2014. Power law for elastic moduli of unsaturated soil. J. Geotech. Geoenviron. Eng. 140 (1), 46–56.
Lu, N., Khorshidi, M., 2015. Mechanisms for soil-water retention and hysteresis at high suction range. J. Geotech. Geoenviron. Eng. 141 (8), 04015032.
Lu, N., Likos, W.J., 2006. Suction stress characteristic curve for unsaturated soil. J. Geotech. Geoenviron. Eng. 132 (2), 131–142.
Maggio, G., Trafford, A., Donohue, S., 2023. Near-surface seismic characterisation of a railway embankment slope using fibre-optic distributed acoustic sensing. In: Copernicus Meetings.
Mahmoodabadi, M., Bryson, L.S., 2021. Direct application of the soil–water characteristic curve to estimate the shear modulus of unsaturated soils. Int. J. Geomechan. 21 (1), 04020243.
Maraschini, M., Foti, S., 2010. A Monte Carlo multimodal inversion of surface waves. Geophys. J. Int. 182 (3), 1557–1566.
Masrouri, F., Bicalho, K.V., Kawai, K., 2008. Laboratory hydraulic testing in unsaturated soils. Geotech. Geol. Eng. 26, 691–704.
Monroy, R., Zdravkovic, L., Ridley, A., 2010. Evolution of microstructure in compacted London Clay during wetting and loading. Géotechnique 60 (2), 105–119.
Mu, Q., Dong, H., Liao, H., Dang, Y., Zhou, C., 2020. Water-retention curves of loess under wetting− drying cycles. Géotechn. Lett. 10 (2), 135–140.
Nyambayo, V., Potts, D., Addenbrooke, T., 2004. The influence of permeability on the stability of embankments experiencing seasonal cyclic pore water pressure changes. In: Advances in Geotechnical Engineering: The Skempton Conference: Proceedings of a Three Day Conference on Advances in Geotechnical Engineering, Organised by the Institution of Civil Engineers and held at the Royal Geographical Society, London, UK, on 29–31 March 2004. Thomas Telford Publishing, pp. 898–910.
Olafsdottir, E.A., Erlingsson, S., Bessason, B., 2018. Tool for analysis of multichannel analysis of surface waves (MASW) field data and evaluation of shear wave velocity profiles of soils. Can. Geotech. J. 55 (2), 217–233.
Ouellet, S.M., Dettmer, J., Lato, M.J., Cole, S., Hutchinson, D.J., Karrenbach, M., Dashwood, B., Chambers, J.E., Crickmore, R., 2024. Previously hidden landslide processes revealed using distributed acoustic sensing with nanostrain-rate sensitivity. Nat. Commun. 15 (1), 6239.
Pasquet, S., Bodet, L., Dhemaied, A., Mouhri, A., Vitale, Q., Rejiba, F., Flipo, N., Guérin, R., 2015. Detecting different water table levels in a shallow aquifer with combined P-, surface and SH-wave surveys: Insights from VP/VS or Poisson's ratios. J. Appl. Geophys. 113, 38–50.
Postill, H., Dixon, N., Fowmes, G., El-Hamalawi, A., Take, W.A., 2020. Modelling seasonal ratcheting and progressive failure in clay slopes: a validation. Can. Geotech. J. 57 (9), 1265–1279.
Rail, N., 2018. Earthworks Technical Strategy. Network Rail, Milton Keynes.
Rail, N., 2011. In: Rail Safety and Standards Board (RSSB) (Ed.), RSSB 1386 (Revised) the Effects of Railway Traffic on Embankment Stability-Final Report.
Reeves, G.M., Sims, I., Cripps, J., 2006. Clay Materials Used in Construction. Geological Society of London.
Ridley, A., McGinnity, B., Vaughan, P., 2004. Role of pore water pressures in embankment stability. Proc. Inst. Civil Eng. Geotechn. Eng. 157 (4), 193–198.
Rossi, M., Wisén, R., Vignoli, G., Coni, M., 2022. Assessment of distributed Acoustic Sensing (DAS) performance for geotechnical applications. Eng. Geol. 306, 106729.
Saneiyan, S., Ntarlagiannis, D., Werkema Jr., D.D., Ustra, A., 2018. Geophysical methods for monitoring soil stabilization processes. J. Appl. Geophys. 148, 234–244.
Saqlain, M., Trafford, A., Khan, Q., Dashwood, B., Chambers, J.E., Jessamy, G., Harms, J., Donohue, S., 2026. Assessment of railway earthworks using DAS based active MASW surveys. Under review.
Shao, J., Wang, Y., Chen, L., 2022. Near-surface characterization using high-speed train seismic data recorded by a distributed acoustic sensing array. IEEE Trans. Geosci. Remote Sens. 60, 1–11.
Šimůnek, J., Kodešová, R., Gribb, M.M., van Genuchten, M.T., 1999. Estimating hysteresis in the soil water retention function from cone permeameter experiments. Water Resour. Res. 35 (5), 1329–1345.
Socco, L.V., Foti, S., Boiero, D., 2010. Surface-wave analysis for building near-surface velocity models — established approaches and new perspectives. Geophysics 75 (5), 75A83–75A102.
Soga, K., Luo, L., 2018. Distributed fiber optics sensors for civil engineering infrastructure sensing. J. Struct. Integr. Maint. 3 (1), 1–21.
Stirling, R.A., Toll, D.G., Glendinning, S., Helm, P.R., Yildiz, A., Hughes, P.N., Asquith, J. D., 2021. Weather-driven deterioration processes affecting the performance of embankment slopes. Géotechnique 71 (11), 957–969.
Subramaniam, P., Yunhuo, Z., Ng, Y.C., Danovan, W., Ku, T., 2020. Modal analysis of Rayleigh waves using classical MASW-MAM approach: Site investigation in a reclaimed land. Soil Dyn. Earthq. Eng. 128, 105902.
Subramanian, S., Khan, Q., Ku, T., 2020. Effect of sand on the stiffness characteristics of cement-stabilized clay. Constr. Build. Mater. 264, 120192.
Take, W., Bolton, M., 2011. Seasonal ratcheting and softening in clay slopes, leading to first-time failure. Géotechnique 61 (9), 757–769.
Thevenet, E., Toubiana, H., Trafford, A., Donohue, S., Harms, J., Bardainne, T., 2024. Assessing 3D slope condition with fibre optic seismic imaging using trains as sources. In: NSG 2024 30th European Meeting of Environmental and Engineering Geophysics, 2024. European Association of Geoscientists & Engineers, pp. 1–5 no. 1.

Trafford, A., Ellwood, R., Wacquier, L., Godfrey, A., Minto, C., Coughlan, M., Donohue, S., 2022. Distributed acoustic sensing for active offshore shear wave profiling. Sci. Rep. 12 (1), 9691.
Trafford, A., Ellwood, R., Godfrey, A., Minto, C., Donohue, S., 2024a. Distributed acoustic sensing for seismic surface wave data acquisition in an intertidal environment. Geophysics 89 (4), 1–35.
Trafford, A., Saqlain, M., Chambers, J., Dashwood, B., Crickmore, R., Harms, J., Donohue, S., 2024b. Seasonal variation in railway embankment condition from passive analysis of train generated surface waves using DAS. In: NSG 2024 30th European Meeting of Environmental and Engineering Geophysics, 2024. European Association of Geoscientists & Engineers, pp. 1–5 no. 1.
Vaughan, P., Kovacevic, N., Potts, D., 2004. Then and now: some comments on the design and analysis of slopes and embankments. In: Advances in Geotechnical Engineering: The Skempton Conference: Proceedings of a three Day Conference on Advances in Geotechnical Engineering, Organised by the Institution of Civil Engineers and held at the Royal Geographical Society, London, UK, on 29–31 March 2004. Thomas Telford Publishing, pp. 241–290.
Wacquier, L., Whiteley, J., Gunn, D., Dashwood, B., Chambers, J., Watlet, A., Trafford, A., Donohue, S., 2021. Time-lapse monitoring of moisture induced landslide using surface waves at Hollin Hill landslide obsevatory. In: NSG2021 27th European Meeting of Environmental and Engineering Geophysics, 2021. European Association of Geoscientists & Engineers, pp. 1–5 no. 1.
Walker, C., Heitor, A., Clarke, B., 2022. Influence of weather-driven processes on the performance of UK transport infrastructure with reference to historic geostructures. Appl. Sci. 12 (15), 7461.
Walker, C., Heitor, A., Clarke, B.G., 2023. Impact of drying-wetting cycles on the small strain behaviour of compacted clay. Transp. Geotechn. 42, 101063.
Xu, X.-T., Jian, W.-B., Wu, N.-S., Xu, X., Shao, L.-J., 2020. Void ratio–dependent water retention model for a deformable residual clay. Int. J. Geomechan. 20 (8), 04020131.
Yamashita, S., Kawaguchi, T., Nakata, Y., Mikami, T., Fujiwara, T., Shibuya, S., 2009. Interpretation of international parallel test on the measurement of Gmax using bender elements. Soils Found. 49 (4), 631–650.
Yesnik, C., Soliman, H., Morozov, I., Fleming, I., Landry, E., 2025. Spatial and temporal changes in small-strain shear modulus of geogrid-stabilized crushed aggregate materials. Transp. Geotechn. 50, 101457.
Zhang, L., Ge, K., Wang, J., Zhao, J., Song, Y., 2020. Pore-scale investigation of permeability evolution during hydrate formation using a pore network model based on X-ray CT. Mar. Pet. Geol. 113, 104157.